Theoretical Chemistry Accounts (2020) 139:95
https://doi.org/10.1007/s00214-020-02604-0

REGULAR ARTICLE

Bonding analysis of the effect of strain on trigger bonds in organic-cage energetic materials

Craig A. Bayse[1] · **Mohammad Jaffar**[1]

Received: 14 January 2020 / Accepted: 6 May 2020 / Published online: 22 May 2020

Abstract

Wiberg bond index and natural bond orbital analyses were used to examine the effect of strain on trigger bonds for a series of organic-cage molecules. In substituted cage hydrocarbons, weakening of the interior C–C bonds and strengthening of exterior C–X bonds are explained in terms of the contributions of the carbon 2*s* and 2*p* atomic orbitals to the bonds. The interior C–C, rather than C–NO_2, bonds are expected to break to initiate explosive decomposition in nitro-substituted tetrahedranes, prismanes, and cubanes. Activation of C–C bonds in cage molecules increases with nitro substitution, but persubstituted cages are not necessarily the most activated. For example, heptanitrocubane is predicted to be more sensitive than octanitrocubane, consistent with experimental studies. In contrast, for a series of hypothetical nitroester substituted prismanes, the strengthening of the exterior C–ONO_2 bond weakens the O–NO_2 bond more than the interior C–C bonds. In CL-20 and TEX, cage strain as determined by WBI analysis in the fused five- and six-membered rings is less significant than for the cage hydrocarbon. In these known energetic materials, the N–NO_2 trigger bonds are activated by the orientation of the nitro groups.

Keywords Density functional theory · Energetic materials · Wiberg bond indices · Cage compounds · Natural bond orbitals

1 Introduction

Understanding the molecular features that lead to explosive decomposition is important for improving the performance of energetic materials (EMs) while lowering their potential environmental impact [1–3]. Explosophores, such as nitro or azide groups, are substituents which facilitate explosive decomposition by incorporating bonds readily broken under conditions of impact, shock, friction, or other stimulative events [4]. Within EMs, the trigger bond is defined as the linkage that breaks to initiate the explosion [5]. These bonds are typically associated with an explosophore and are weakened, or activated, toward cleavage. For example, in nitro-based EMs, a C–NO_2 is often the trigger bond. In organic cage compounds, energetic properties are additionally influenced by strained bonds that lead to high heats of formation and compact structures [6].

Examples of known organic-cage EMs include hexaazaisowurtzitane-based CL-20 and the structurally related explosive TEX (Fig. 1). The primary application of CL-20, proposed in 1979 and synthesized for the first time at the China Lake weapons development facility, is as a military propellant because it produces less visible smoke as it burns. Cage hydrocarbons have been considered as potential EMs due to the energy stored in their highly strained bonds. Tetrahedrane, with the highest strain energy (571.9 kJ/mol [7]), has never been synthesized. Prismane, or Ladenburg benzene, is explosively unstable (strain energy = 606.9 kJ/mol [7]) and computational studies show its nitro derivatives would have large positive heats of formation [8, 9]. Cubane is also a known molecule for which nitro derivatives heptanitrocubane (HNC) and octanitrocubane (ONC) have been synthesized as potential EMs with exceptional energy density [10, 11].

Various groups have used computational methods to examine the energetic properties of substituted tetrahedranes [12–15], prismanes [8, 12, 14, 16, 17], cubanes [18–26], hexaazaisowurtzitane-like derivatives [25, 27–40], and other strained EMs [41–49]. These studies have used a variety of

Electronic supplementary material The online version of this article (https://doi.org/10.1007/s00214-020-02604-0) contains supplementary material, which is available to authorized users.

✉ Craig A. Bayse
cbayse@odu.edu

[1] Department of Chemistry and Biochemistry, Old Dominion University, Norfolk, VA 23529, USA

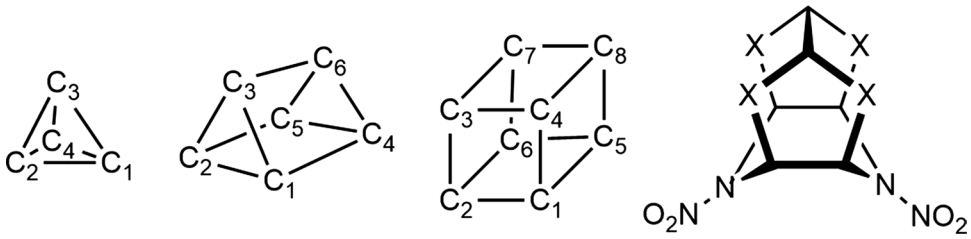

Fig. 1 Selected known and hypothetical organic cage energetic materials: tetrahedranes (**1**), prismanes (**2**), cubanes (**3**), CL-20 (X = N–NO_2), and TEX (X = O)

methods including bond dissociation energies (BDEs), atoms-in-molecules models, electrostatic potentials, distributed multipole analysis, and other computational methods in both the gas and condensed phases to examine bonding in EMs.

$$\%\Delta \mathrm{WBI_{AB}} = \frac{\mathrm{WBI_{AB}(EM)} - \mathrm{WBI_{AB}(reference)}}{\mathrm{WBI_{AB}(reference)}} \times 100 \quad (1)$$

Wiberg bond index (WBI) analysis [50] is an alternate tool used by various groups to identify trigger bonds in EMs [51–57]. WBIs are a convenient measure of electron density between two atoms in a bond and have an advantage over BDEs in that they measure the bond strength of the intact bond and do not require open-shell calculations of molecular fragments. As a means to determine the effect of the chemical environment on potential trigger bonds, relative percent changes in WBIs (%ΔWBIs, Eq. 1) are calculated for target molecules and compared to bonds in reference molecules with the same bond type, hybridization, and explosophore for a relative scale of the bond strength. Trigger bonds are assigned for individual molecules based on the value of %ΔWBI. Negative %ΔWBIs indicate a bond with lower electron density, and higher susceptibility to breaking, than a reference bond. Conversely, positive %ΔWBIs points to bonds strengthened versus the reference bond.

In this study, WBI analysis is applied to several classes of organic cage compounds to determine the effect of strain on the composition and assignment of trigger bonds. These results are supplemented with natural bond orbital (NBO) analysis [58, 59] to examine how changes in hybridization affect bond strength. Trends for nitro-substituted tetrahedrane, prismane, and cubane cage hydrocarbons show that high strain shifts the trigger bond from the nitro group to the cage itself, consistent with results from other computational methods for bond analysis. In the less-strained cages of known EMs CL-20 and TEX, the strength of the N–NO_2 trigger bonds is influenced by axial or equatorial positioning of the nitro group.

2 Computational methods

Geometries of organic-cage compounds were optimized using Gaussian 09 [60] and the hybrid functional M06-2X with the TZVP [61] and def2-TZVPP [62] basis sets. The DFT(M06-2x)/TZVP level performed well for geometry optimizations of a test set of EMs relative to a selection of basis sets and functionals [51]. Geometries and WBIs in the larger def2-TZVPP basis set are similar to those obtained at the TZVP level, which are reported in the Supporting Information. The augmentation of the TZVP basis set with diffuse functions was found to produce spurious results for WBIs [53]. These functions can be omitted with no significant difference in the optimized geometries versus the standard TZVP basis set. Structures were characterized as minima on the potential energy surface through vibrational analysis. WBIs and NBO bond compositions were calculated using NBO 3.1 [63] from the optimized structures. WBIs were compared to reference molecules to determine the %ΔWBIs by Eq. (1). Generally, reference molecules are selected to have a similar chemical environment to the bond of interest. References selected for **1**–**3** were ethane or the unsubstituted cage molecules (C(sp^3)–C(sp^3)), nitrocyclohexane (C(sp^3)–NO_2), and cyclohexyl nitrate (C(sp^3)–ONO_2 and O(sp^3)–NO_2). Cyclohexyl groups were used instead of methyl to partially preserve the effects of extended C–C bonding at the carbon center. For CL-20 and TEX, *N*,*N*-dimethylnitroamine (DMNA) was the reference for the N(sp^3)–NO_2 bonds. Note that the selection of reference molecule will affect the estimate of the activation of the trigger bond, but the overall trends in relative bond strength will be the same.

3 Results and discussion

3.1 Tetrahedranes, prismanes, and cubanes

The DFT(M06-2X)/def2-TZVPP optimized structures are in good agreement with previous computational studies (i.e., [12–14]) and calculations at the DFT(M06-2X)/TZVP level (see Supporting Information). WBI and NBO analyses were performed from the DFT(M06-2X)/def2-TZVPP optimized geometries of a series of tetrahedrane **1**, prismane **2**, and cubane **3** derivatives to determine the effect of increased nitro substitution on bond strength. The bonds of the hydrocarbon cages are strained by their restrictive interior C–C–C angles which deviate from the ideal 109.47° sp^3 angle. The AOs of an ideal sp^3 center contribute equally to a bond

(contributions for s-type = 25%, total p-type = 75%) and the sum of the contributions for an atom must add to 100%, such that an increase in the contribution of an AO to one bond must reduce its contributions to other bonds. Small cage angles require an increase the contribution of p-type AOs to accommodate the small interior C–C bonds. This effect shifts a larger 2*s* contribution to the exterior C–X bonds. Additionally, the inability of the hybrid orbitals of the cage atoms to overlap effectively decreases the interatom electron density to result in weakened interior C–C bonds due to the curvature in the bond paths [64].

NBO analysis was used to calculate the AO contributions to localized two-center bonds in the cage molecules (Table 1). The effectiveness of the overlap to the interatomic electron density was estimated by %ΔWBIs. In **1**, the cage with the tightest interior bond angles (∠C–C–C = 60°), there is an 80% 2*p* contribution to the C–C bonds, which are 5.96% weaker than ethane. The rectangular face bonds of **2** experience less strain (%ΔWBI = − 5.12%) due to their 90° bond angles and have AO contributions more similar to sp^3. However, the bonds of the triangular faces are more strained than in **1** (%ΔWBI = − 6.12%) due to the shift of 2*s* character to the bonds of the rectangular faces. Bond strain is further reduced in **3** where contributions from C approach sp^3 hybridization, but the 90° angles prevent effective overlap resulting in a weaker bond than ethane (%ΔWBI = − 4.84%). The high contributions of 2*p* to the C–C bonds of **1**–**3** increase the proportion of 2*s* to their exterior C-H bonds, but the admixture decreases as the cages are less strained. The effective overlap and lower contribution from the C 2*s* lead to stronger exterior C-H and C–NO_2 bonds along the series (**1** < **2** < **3**, Tables 1 and 2) albeit with lengthening bond distances [i.e., $\mathbf{1}_1$ (1.424 Å) < $\mathbf{2}_1$ (1.432 Å) < $\mathbf{3}_1$ (1.466 Å)] due to the increase in the admixture of C 2*p*. The weakening of the C–NO_2 bonds is in agreement with the trends in lower BDE for the series of nitro-substituted prismanes [8].

Weak C–NO_2 bonds introduced through the nitro explosophore are important to the energetic capacity of aromatic EMs. However, in monosubstituted cage molecules these bonds are stronger than the typical C(sp^3)–NO_2 bond due to the 2*s* contribution to the exterior C–X bonds. Compared to $CyNO_2$, the C–NO_2 bond is 7.61% stronger in $\mathbf{1}_1$, 8.12% stronger in $\mathbf{2}_1$, and 2.83% stronger in $\mathbf{3}_1$. [Note that trends in the tetrahedranes are anomalous due to significant changes in the cage structure with substitution.] Additional nitro substitutions weaken the C–NO_2 bonds versus the monosubstituted cages with the largest effect observed in the smaller, more strained cages due to greater contributions of the C 2*s* to the bond (Fig. 2a). The overall carbon contribution to the C–NO_2 increases with the C 2*s* character and correlates with weakening of the bond (Fig. 2b). Trendlines differ for each cage molecule due to the differences in the hybridization at the vertex atoms. However, the bonds are stronger than the $CyNO_2$ reference, even at high substitution. In comparison, bonds to nitro groups in several known EMs (TNT, RDX, and HMX) are weaker than their reference bonds in a previous study [51].

%ΔWBI analysis shows that nitro substitution has a more significant effect on the interior cage C–C bonds, especially for the highly strained tetrahedranes (Fig. 3). Even when the parent and mononitro cage hydrocarbons are used as references for the C–C and C–NO_2 bonds, the C–C bonds are generally more activated than C–NO_2. The C–NO_2 bond is weakened by a maximum of − 6.70% in $\mathbf{1}_{1,2,3,4}$, − 5.72% in $\mathbf{2}_{1,2,3,4,5}$, and − 1.36% in ONC versus the monosubstituted parent. Activation of the C–C bonds versus the parent (Table 2) exceeds that of C–NO_2 in all cases), with the single exception of $\mathbf{2}_{1,2,3,4,5,6}$ [%ΔWBI = − 5.37% (C–NO_2 versus $\mathbf{2}_1$); − 5.10% (C–C versus **2**)] where C–NO_2 cleavage could compete with that of the C–C bond. The more favorable activation of C–C bonds in nitro-substituted **1**–**3** is consistent with initial cleavage of these bonds in the previous theoretical calculations and the isomerization of ONC and HNC to annulenes in molecular dynamics simulations [24, 65, 66]. This conclusion does not imply that the nitro groups do not contribute to explosive decomposition, but that they are not predicted to necessarily initiate decomposition. In contrast, an examination of the bond critical points in the series of nitro-substituted tetrahedranes concluded that the weakening of the C–NO_2 bonds with increased substitution was greater than the C–C bond [13].

In the tetrahedrane series, the first nitro group weakens the adjacent C–C bond by 11.5% versus **1**. The nitro groups in $\mathbf{1}_{1,2}$ twist to distort the cage in C_2 symmetry, which weakens two bonds to the –CH fragment by 19.3% versus cyclohexane (Table 2). $\mathbf{1}_{1,2,3}$ flattens into a kite-like structure with C–C bonds on opposite edges of the cage lengthening to over 1.63 Å (Table 2). The bonds in $\mathbf{1}_{1,2,3,4}$ are slightly

Table 1 Contributions of carbon atomic orbitals to the NBOs of cage hydrocarbons calculated at the DFT(M06-2X)/def2-TZVPP level

	C–H					C_{tri}–C_{tri}				C_{sq}–C_{sq}			
	d(C–H) (Å)	WBI	*%C*	*%s*	*%p*	*d*(C–C) (Å)	WBI	*%s*	*%p*	*d*(C–C) (Å)	WBI	*%s*	*%p*
1	1.068	0.905	63.4	40.0	60.0	1.467	0.984	19.9	80.0				
2	1.078	0.916	62.1	33.4	66.6	1.511	0.982	19.7	80.1	1.548	0.992	26.9	73.0
3	1.085	0.924	61.2	30.3	69.7					1.560	0.995	23.2	76.7

Table 2 Assignment of trigger bonds for nitro-substituted **1**–**3** from WBI analysis calculated at the DFT(M06-2X)/def2-TZVPP level

	Isomer	Trigger bond	*d*(C–C) (Å)	WBI	%ΔWBI[a]	%ΔWBI[b]	Δ*E*+ZPE[c]
1	1	C1–C2	1.487	0.902	−11.45	−8.32	
	1,2	C1–C3	1.568	0.822	−19.26	−16.40	
	1,2,3	C1–C2	1.631	0.754	−25.96	−23.34	
	1,2,3,4	C1–C2	1.683	0.728	−28.55	−26.03	
2	1	C1–C2	1.512	0.927	−8.97	−5.58	
	1,2	C1–C2	1.513	0.928	−11.53	−8.24	5.33
	1,4	C1–C2	1.513	0.928	−8.86	−5.47	4.02
	1,5	C1–C2	1.513	0.929	−8.81	−5.42	0.00
	1,2,3	C1–C2	1.508	0.930	−8.67	−5.28	8.54
	1,2,4	C1–C2	1.515	0.909	−10.74	−7.42	3.17
	1,2,6	C1–C2	1.519	0.910	−10.61	−7.29	0.00
	1,2,3,4	C1–C2	1.517	0.922	−9.48	−6.11	3.11
	1,2,4,5	C1–C2	1.509	0.919	−9.72	−6.37	3.60
	1,2,4,6	C1–C2	1.516	0.912	−10.50	−7.17	0.00
	1,2,3,4,5	C4–C6	1.511	0.921	−9.54	−6.18	
	1,2,3,4,5,6	C1–C2	1.508	0.932	−8.50	−5.10	
3	1	C1–C2	1.559	0.959	−5.79	−3.61	
	1,2	C1–C2	1.542	0.955	−6.25	−4.08	2.79
	1,3	C1–C2	1.555	0.965	−5.28	−3.08	1.17
	1,7	C1–C2	1.554	0.967	−5.09	−2.88	0.00
	1,2,3	C1–C2	1.547	0.949	−6.81	−4.65	3.44
	1,3,4	C3–C4	1.543	0.955	−6.23	−4.05	1.32
	1,3,6	C3–C4	1.562	0.959	−5.88	−3.70	0.00
	1,2,3,4	C1–C2	1.546	0.952	−6.57	−4.40	7.79
	1,2,3,5	C1–C2	1.552	0.946	−7.42	−5.27	3.87
	1,2,3,7	C1–C2	1.546	0.948	−6.87	−4.71	5.45
	1,2,3,8	C1–C2	1.549	0.948	−6.88	−4.72	2.51
	1,3,5,7	C1–C5	1.545	0.955	−6.21	−4.03	1.79
	1,3,6,8	C1–C2	1.561	0.959	−5.85	−3.67	0.00
	1,2,3,4,5	C1–C5	1.547	0.948	−6.94	−4.78	3.10
	1,2,3,5,7	C1–C2	1.551	0.947	−7.06	−4.90	0.37
	1,2,3,6,8	C2–C6	1.549	0.947	−6.98	−4.82	0.00
	1,2,3,4,5,6	C1–C5	1.550	0.947	−7.01	−4.85	3.11
	1,2,3,4,5,7	C1–C2	1.550	0.947	−7.05	−4.90	0.75
	1,2,3,5,7,8	C1–C5	1.550	0.946	−7.12	−4.96	0.00
	1,2,3,4,5,6,7	C1–C2	1.551	0.943	−7.40	−5.25	
	1,2,3,4,5,6,7,8	C1–C2	1.553	0.944	−7.32	−5.16	

[a]%ΔWBI calculated versus cyclohexane

[b]%ΔWBI calculated versus the parent cage hydrocarbon

[c]Relative energies corrected for zero-point energy contributions (Δ*E*+ZPE) are given when multiple substitutional isomers are possible

longer and weakened by 28.6% relative to **1**. For prismanes and cubanes, the position of the substitutions influences the stability of the isomers and which C–C bonds are most activated (Table 2). Isomers with the most spacing between nitro groups tend to be the lowest energy structures (i.e., $\mathbf{2_{1,5}}$ and $\mathbf{2_{1,2,6}}$; $\mathbf{3_{1,7}}$ and $\mathbf{3_{1,3,6,8}}$). Nitro groups on adjacent positions activates the C–C bond due to steric interactions in addition to inductive effects ($\mathbf{2_{1,2,4,6}}$ and $\mathbf{3_{1,2,3,5}}$). Surprisingly, $\mathbf{2_{1,2,3}}$ in which the nitro groups are most crowded is the least activated trinitroprismane due to the depletion of electron density in the triangular face. Highly substituted $\mathbf{2_{1,2,3,4,5}}$ (PNP) and hexanitroprismane (HNP) are also less activated than would be expected from the steric repulsions between their nitro groups. Penta- and hexasubstituted cubanes have similar C–C %ΔWBIs and are less activated (~ − 7.0%) than prismanes with similar number of nitro groups due to the

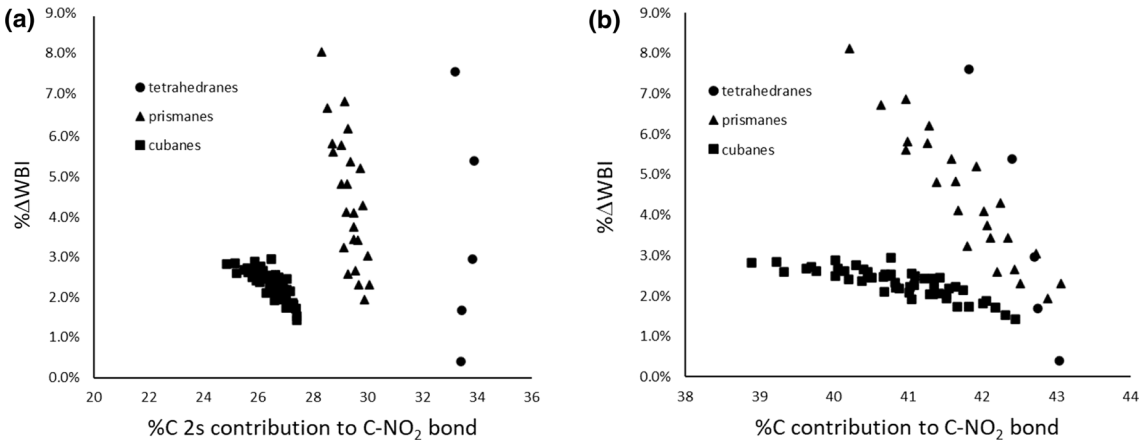

Fig. 2 Correlation of the percentage of **a** the C 2*s* contribution and **b** the overall C contribution to the C–NO_2 bond with its bond strength as measured by the %ΔWBI calculated relative to the C(sp^3)–NO_2 bond of nitrocyclohexane. Note: the anomalous trend for tetrahedranes in (**a**) is due to distortions in the C_4 cage with high substitution

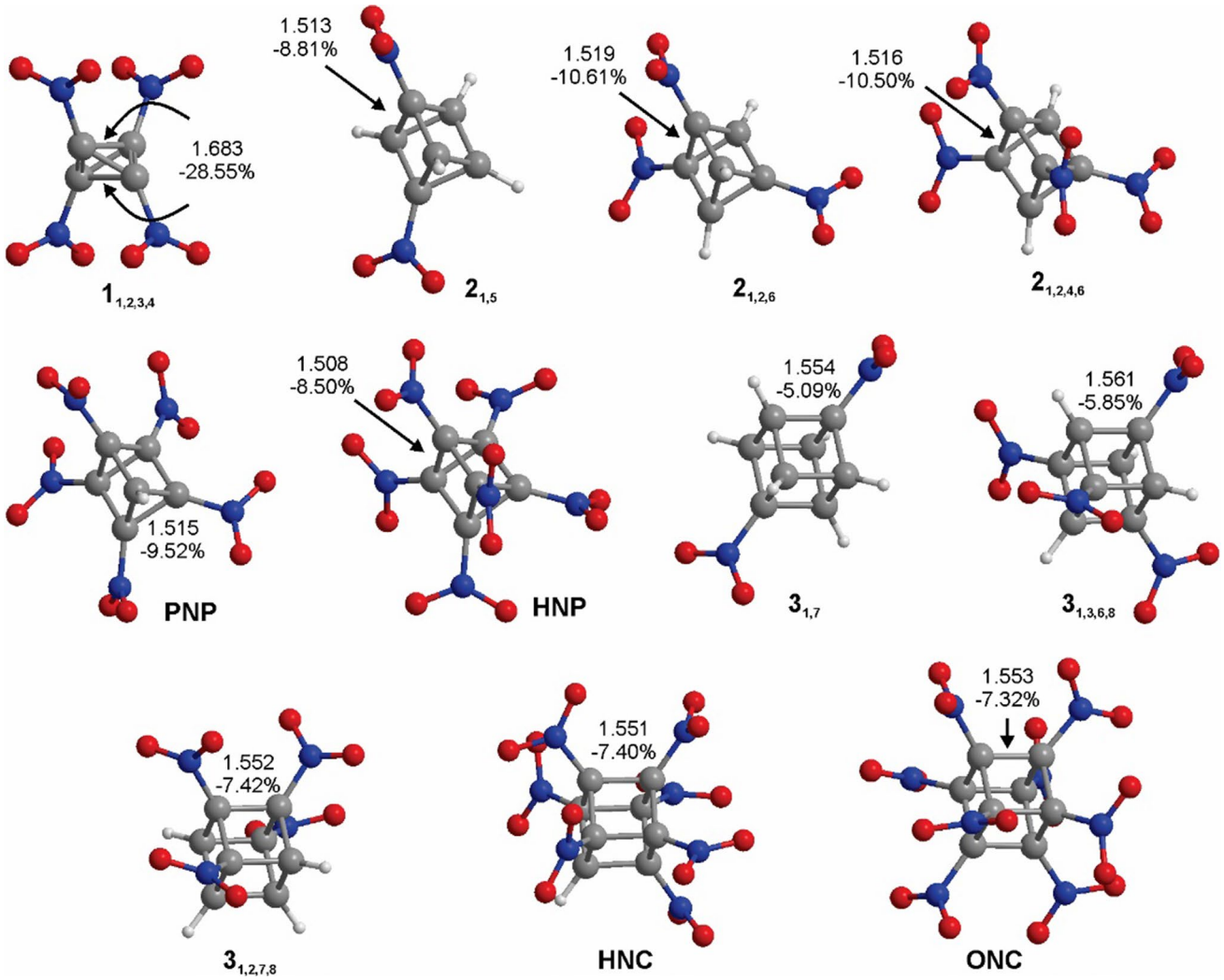

Fig. 3 DFT(M06-2X)/def2-TZVPP bond distances (Å) and relative WBI bond strengths (%ΔWBI) versus nitrocyclohexane for C(sp^3)–NO_2 bonds in selected nitro-substituted **1**–**3**

lower cage strain. These trends are consistent with previous studies of the effect of substitution on the electrostatic potential and electron density of cage molecules [20].

In the fully substituted cage molecules, the trend in the C–C bond strength follows the strain of the cage (**1** > **2** > **3**). However, for **2** and **3**, the persubstituted derivative is not predicted to have the most sensitive C–C bond. Both PNP and HNC are slightly more sensitive than HNP or ONC. In PNP, the C1–C3 trigger bond is weakened by the redistribution of the C1 AOs to increase its 2*s* contribution to the C_3–C_6 rectangular face bond. For HNC, the absence of a nitro group allows repulsions between the groups bonded opposite the CH–CNO_2 weaken the bond. This result contrasts with other studies that suggest that ONC is more activated [20] and may point the possibility that HNC would be a more sensitive EM.

3.2 Prismane nitroesters

A series of nitroester prismane compounds proposed by Chi and Li [17] were optimized for comparison to their nitro analogues. Most low energy conformations orient the –NO_2 groups toward the –CH vertices. Substitutions on opposite corners of rectangular faces have their nitro groups oriented coplanar. The increased C 2*s* character of the exterior C–ONO_2 bonds strengthens these bonds relative to the reference $CyONO_2$ molecule by 9–17% (Table 3). The ester O concentrates its 2*s* AO to match the strengthened C–ONO_2 bond which depletes the 2*s* contributions to the O–NO_2 bond, which is weakened by 8–17%. As a result, the increase in the C 2*s* contribution to the C–ONO_2 bond correlates with an weakening of the O–NO_2 bond (Fig. 4a) These results are consistent with previous studies showing a lower BDE for the O–NO_2 bond [17]. Comparison of the %ΔWBI to reported H_{50} estimates [17] of the impact sensitivity indicates that the %ΔWBI for the O(sp^3)–NO_2 bond correlate with the predicted sensitivity of the material (Fig. 4b). The C–C bonds are also weakened with increased nitroester substitution, but, unlike the nitro derivatives, the O–NO_2 bonds are generally weaker and are assigned as the trigger bonds for this class of molecules (Fig. 5). However, nitroester substitutions on adjacent carbons of the triangular faces can significantly activate the C–C bonds (%ΔWBI = 10–13%) and exceed those of the nitro derivatives due to the depletion of electron density by the strong C–ONO_2 bonds. As a result, cleavage of these bonds could compete with O–NO_2 bond breakage. These highly substituted nitroester prismanes are predicted to be highly unstable if they could be synthesized.

3.3 CL-20 and TEX

The hexaazaisowurzitane cage of CL-20 cage is less strained than **1**–**3** due to the puckering of its 5-, 6-, and 7-membered rings to bond angles closer to the sp^3 ideal. CL-20 consists of two C–C bonded imidazolidine rings fused to a boat piperazine (Pip) base. N(sp^3)–NO_2 bonds are found at each nitrogen of the heterocage molecule. Multiple conformations are available due to the axial or equatorial positioning of the nitro groups with respect to the Pip ring and the seven-membered 1,3,5-triazepane (Tri) rings. Various previous computational studies have established the N–NO_2 bond as key to explosive decomposition in this class of EM [35–37]. The eight conformations of CL-20 from Kholod et al. [29] corresponding to structures found in the four crystalline polymorphs (α and γ(**II**), β(**IV**), ε(**III**), ζ(**I**)) were optimized at the DFT(M06-2X/TZVP) level. Conformation **IV** is the most stable conformation in the gas phase (Table 4).

Table 3 Trigger bonds for nitroester-substituted **2E** calculated at the DFT(M06-2X)/def2-TZVPP level

Isomer	Position	*d*(C–O) (Å)	WBI	%ΔWBI C–ONO_2	*d*(O–N) (Å)	WBI	%ΔWBI O–NO_2	ΔE + ZPE[a]
1	C1	1.376	0.959	9.60%	1.415	0.865	− 7.95	
1,2	C1	1.368	0.980	12.01%	1.429	0.839	− 10.72	1.84
1,4	C1	1.369	0.976	11.52%	1.425	0.846	− 9.98	1.45
1,5	C1	1.374	0.965	10.27%	1.420	0.856	− 8.87	0.00
1,2,3	C1	1.361	0.997	13.94%	1.439	0.819	− 12.80	2.69
1,2,4	C1	1.361	0.996	13.83%	1.438	0.822	− 12.50	0.69
1,2,6	C1	1.366	0.984	12.42%	1.431	0.834	− 11.25	0.00
1,2,3,4	C1	1.355	1.012	15.63%	1.450	0.802	− 14.62	1.25
1,2,4,5	C1	1.360	1.002	14.50%	1.445	0.810	− 13.84	0.91
1,2,4,6	C1	1.360	1.000	14.24%	1.442	0.815	− 13.22	0.00
1,2,3,4,5	C2	1.353	1.017	16.26%	1.456	0.789	− 15.98	
1,2,3,4,5,6	C1	1.353	1.018	16.37%	1.458	0.786	− 16.33	

[a]Relative energies corrected for zero-point energy contributions (ΔE + ZPE) are given when multiple substitutional isomers are possible

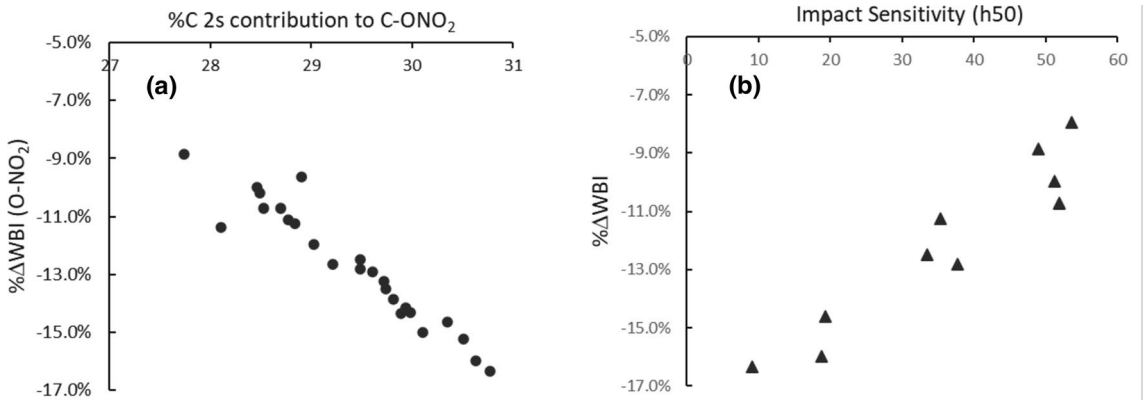

Fig. 4 **a** Correlation of the percentage of C 2*s* contribution to the C–ONO_2 bonds of **2E** with the O–NO_2 strength as measured by the %ΔWBI calculated relative to the O(sp^3)–NO_2 bond of cyclohexyl nitrate. **b** Comparison of %ΔWBI for the O(sp^3)–NO_2 bond to the estimated impact sensitivity (h_{50}) as determined in reference [17]

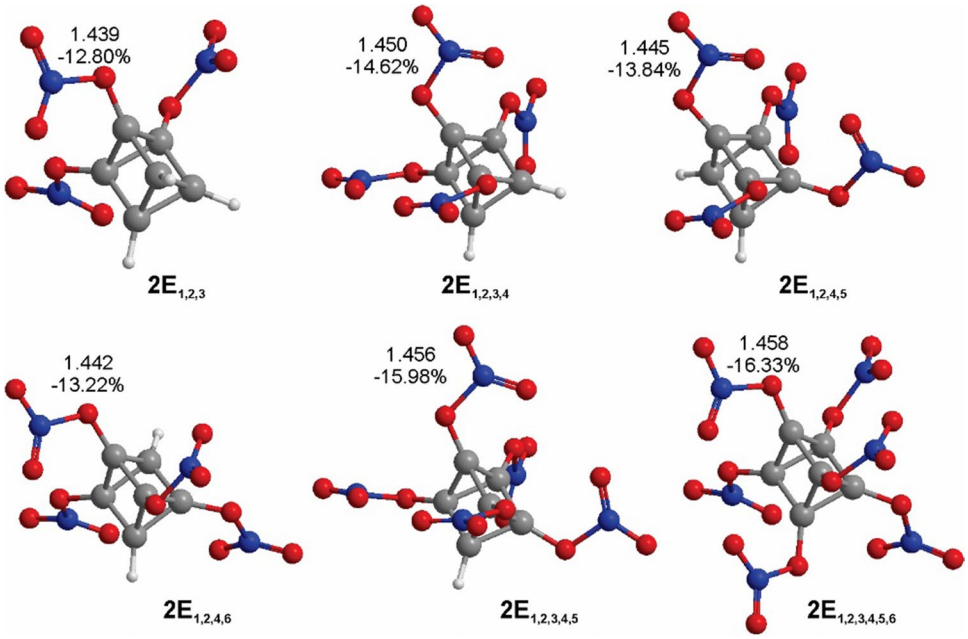

Fig. 5 DFT(M06-2X)/def2-TZVPP bond distances (Å) and relative WBI bond strengths (%ΔWBI) versus cyclohexyl nitroester for O(sp^3)–NO_2 bonds in selected prismane nitroesters

WBI analysis shows that the most activated N–NO_2 bonds are 10–11% weaker than the *N,N*-dimethylnitramine (DMNA) reference compound, but the differences between the conformations are small (Table 4). Nitro groups in the equatorial positions tend to be more activated (%ΔWBI = 8.5–12.0%) than the axial positions (%ΔWBI = 4.0–7.5%) due to the increased steric interactions in the former. These results are consistent with sensitivity trends predicted by vibrational frequency analysis at the MBPT(2) level [37]. Bond activation correlates with the %s contribution of the ring nitrogen of the N–NO_2 bond (Fig. 6) with the trends for the triazepane nitro groups different than for the piperazines due to the ring strain in the six- and seven-membered rings. For **IVa**, the equatorial N–NO_2 on the triazepane ring is weaker than on the piperazine consistent with relative BDEs calculated at the DFT(B3LYP)/cc-pVTZ//DFT(B3LYP)/6-31 g* level (37.6 versus 41.1 kcal/mol) [28]. Comparison of the predicted most activated bonds does not correlate with the experimental trend in sensitivity ($\varepsilon > \gamma > \alpha > \beta, \zeta$). The differences in bond strength are small between the conformations suggesting a significant contribution from intermolecular interactions within the polymorphs.

Substitution of four imidazolidine N–NO_2 groups with O for the EM TEX decreases the steric interaction of nitro groups (Table 4) and the activation of the trigger bonds relative to CL-20 by 2–3%. The exo-exo conformation is 3.32 kcal/mol more stable than the exo-endo. The N–NO_2 bonds are less activated than CL-20, consistent with the lower sensitivity of TEX. Generally, substitutions of the

Table 4 Trigger bonds for Cl-20 and TEX (For atom numbering, see Fig. 6) and relative energies corrected for zero-point energy contributions ($\Delta E + ZPE$) calculated at the DFT(M06-2X)/def2-TZVPP level

	Conformer	Location of trigger bond			d(N–N) (Å)	WBI	%ΔWBI	$\Delta E + ZPE$[a]
I		$N_5 = N_6$	Pip	eq	1.416	0.941	− 10.65	4.26 (2.30)
II	a	N_4	Tri	eq	1.425	0.934	− 11.27	2.18 (1.13)
	b	N_5	Pip	eq	1.418	0.931	− 11.60	3.46 (1.27)
	c	N_6	Pip	eq	1.423	0.931	− 11.61	3.06 (1.27)
III	a	$N_1 = N_2$	Tri	eq	1.422	0.935	− 11.24	1.28 (1.69)
	b	N_6	Pip	eq	1.417	0.932	− 11.47	1.66 (1.67)
IV	a	$N_1 = N_4$	Tri	eq	1.426	0.929	− 11.72	0.00 (0.00)
	b	N_4	Tri	eq	1.427	0.929	− 11.81	0.71 (6.15)
TEX	a	$N_5 = N_6$	Pip	eq	1.408	0.962	− 8.60	0.00
II	b	N_6	Pip	eq	1.414	0.953	− 9.52	3.32

[a]Parenthetical $\Delta E + ZPE$ values (DFT(B3LYP)/6-31+G**) are from ref [29]

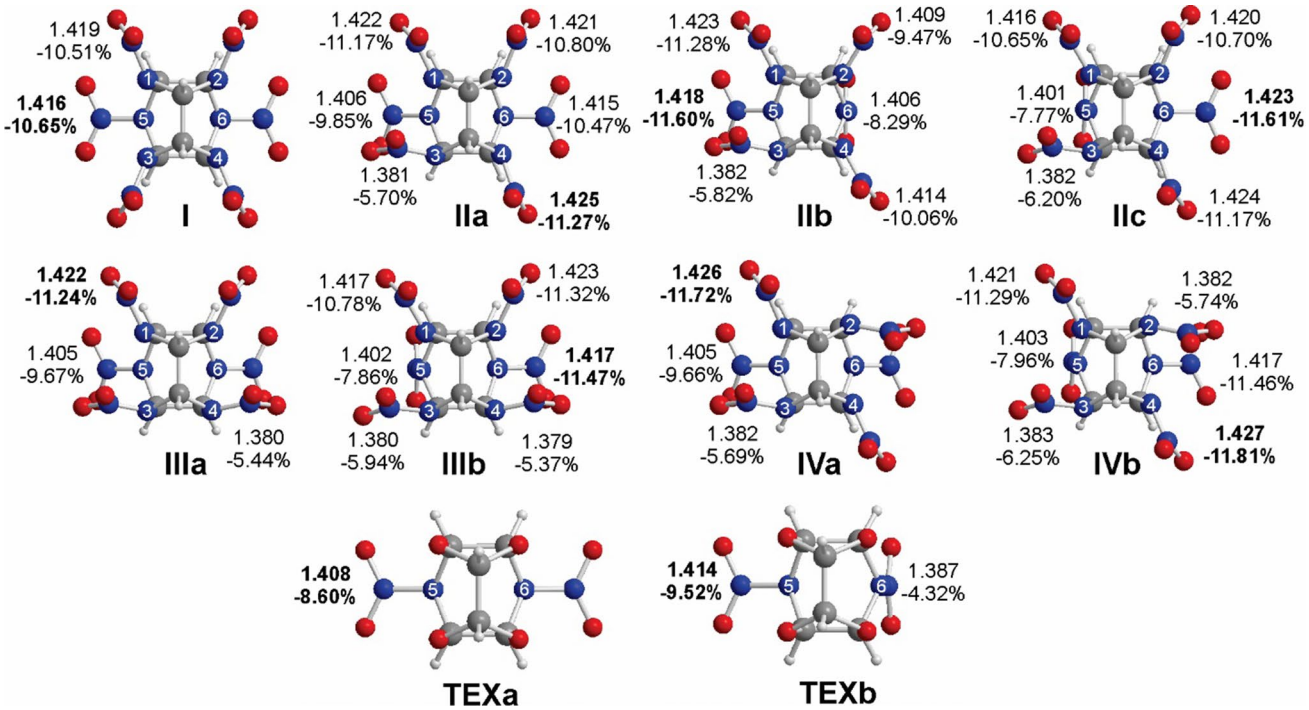

Fig. 6 DFT(M06-2X)/def2-TZVPP bond distances (Å) and relative WBI bond strengths (%ΔWBI) versus DMNA for N–NO_2 bonds in conformers of CL-20 and TEX. Trigger bond assignments are in bold font

N–NO_2 groups with oxygen centers lead to the less sensitive materials [34].

4 Conclusions

Trigger bonds were assigned to organic-cage energetic materials by comparing the bond strengths to analogous bonds in reference molecules. Generally, trigger bonds are assumed to be the bond most susceptible to breaking under stress to initiate explosive decomposition. These bonds have lower electron densities as measured by the Wiberg bond index. For substituted cage hydrocarbons, strain focuses the C 2*p* contribution to the interior C–C cage bonds while increasing the C 2*s* contribution to the exterior C–X bond. As a result, the exterior C–NO_2 bonds are stronger than in nitro-substituted aromatics and the interior C–C bonds are weakened. Therefore, the latter are assigned as the trigger bonds for tetrahedrane, prismane, and cubane classes of potential energetic materials. Only in the case of the pentasubstituted prismane could C–NO_2 cleavage be expected to act as the trigger bond. In nitroester substituted prismanes, the strengthening of the C–ONO_2 exterior bonds due to strain weakens the O–NO_2 bond to a greater extent than the C–C

bonds, although both bond types are predicted to be activated in highly substituted derivatives. In CL-20 and TEX, the cage strain is not as significant as the hydrocarbons such that the exterior N–NO_2 bonds are assigned as the trigger bonds. The activation of these bonds is dependent upon their orientation in the fused five- and six-membered rings of the molecule. These results provide additional support for the use of Wiberg bond index analysis to predict the molecular properties of energetic materials which will assist in the development of future novel materials.

5 Supporting information

Selected structural information for DFT(M06-2X)/TZVP-optimized geometries. Cartesian coordinates of DFT(M06-2X)/TZVP-optimized geometries.

Acknowledgements M.J. was supported through an NSF-REU site (CHE-1659476). Calculations were performed on the Turing High Performance Cluster maintained by ODU Information Technology Services.

References

1. Talawar MB, Sivabalan R, Mukundan T et al (2009) Environmentally compatible next generation green energetic materials (GEMs). J Haz Mat 161:589–607. https://doi.org/10.1016/j.jhazmat.2008.04.011
2. Giles J (2004) Green explosives: collateral damage. Nature 427:580–581. https://doi.org/10.1038/427580a
3. Witze A (2013) Green fuels blast off. Nature 500:509–510. https://doi.org/10.1038/500509a
4. Yin P, Zhang Q, Shreeve JM (2016) Dancing with energetic nitrogen atoms: versatile N-functionalization strategies for *N*-heterocyclic frameworks in high energy density materials. Acc Chem Res 49:4–16. https://doi.org/10.1021/acs.accounts.5b00477
5. Kamlet M, Adolph H (1979) Relationship of impact sensitivity with structure of organic high explosives. 2. Polynitroaromatic explosives. Propellants Explos 4:30–34. https://doi.org/10.1002/prep.19790040204
6. Sikder AK, Maddala G, Agrawal JP, Singh H (2001) Important aspects of behaviour of organic energetic compounds: a review. J Haz Mat 84:1–26. https://doi.org/10.1016/S0304-3894(01)00178-9
7. Novak I (2003) Substituent effects on steric strain. Chem Phys Lett 380:258–262. https://doi.org/10.1016/j.cplett.2003.08.109
8. Chi W-J, Li L-L, Li B-T, Wu H-S (2012) Density functional calculations for a high energy density compound of formula $C_6H_{6-n}(NO_2)_n$. J Mol Model 18:3695–3704. https://doi.org/10.1007/s00894-012-1367-6
9. Chi W-J, Li L-L, Li B-T, Wu H-S (2013) Theoretical investigation on detonation performances and thermodynamic stabilities of the prismane derivatives. J Mol Model 19:1049–1057. https://doi.org/10.1007/s00894-012-1648-0
10. Zhang M-X, Eaton PE, Gilardi R (2000) Hepta- and octanitrocubanes. Angew Chem Int Ed 39:401–404. https://doi.org/10.1002/(SICI)1521-3773(20000117)39:2%3c401:AID-ANIE401%3e3.0.CO;2-P
11. Eaton PE, Zhang M-X, Gilardi R et al (2002) Octanitrocubane: a new nitrocarbon. Propellants Explos Pyrotech 27:1–6. https://doi.org/10.1002/1521-4087(200203)27:1%3c1:AID-PREP1%3e3.0.CO;2-6
12. Politzer P, Seminario JM (1989) Computational determination of the structures and some properties of tetrahedrane, prismane, and some of their aza analogs. J Phys Chem 93:588–592. https://doi.org/10.1021/j100339a019
13. Zhou G, Zhang J-L, Wong N-B, Tian A (2004) Computational studies on a kind of novel energetic materials tetrahedrane and nitro derivatives. J Mol Struct Theochem 668:189–195. https://doi.org/10.1016/j.theochem.2003.10.054
14. Politzer P, Seminario JM (1989) Computational analysis of the structures, bond properties, and electrostatic potentials of some nitrotetrahedranes and nitroazatetrahedranes. J Phys Chem 93:4742–4745. https://doi.org/10.1021/j100349a013
15. Rayne S, Forest K (2011) A G4MP2 and G4 theoretical study into the thermochemical properties of explosophore substituted tetrahedranes and cubanes. Propellants Explos Pyrotech 36:410–415. https://doi.org/10.1002/prep.201000165
16. Joshi KA, Gejji SP (2005) Molecular electrostatic potentials and electron densities in nitrotriprismanes. J Mol Struct Theochem 724:87–93. https://doi.org/10.1016/j.theochem.2005.02.050
17. Chi W-J, Li Z-S (2015) Molecular design of prismane-based potential energetic materials with high detonation performance and low impact sensitivity. C R Chim 18:1270–1276. https://doi.org/10.1016/j.crci.2015.06.018
18. Murray JS, Seminario JM, Politzer P (1991) Effects of the simultaneous presence of nitro and amine substituents in cubane and some azacubanes. Struct Chem 2:153–166. https://doi.org/10.1007/BF00676627
19. Kortus J, Pederson MR, Richardson SL (2000) Density functional-based prediction of the electronic, structural, and vibrational properties of the energetic molecule: octanitrocubane. Chem Phys Lett 322:224–230. https://doi.org/10.1016/S0009-2614(00)00425-5
20. Gejji SP, Patil UN, Dhumal NR (2004) Molecular electrostatic potentials and electron densities in nitrocubanes $C_8H_{8-\alpha}(NO_2)\alpha$ ($\alpha = 1$–8): ab initio and density functional study. J Mol Struct THOECHEM 681:117–127. https://doi.org/10.1016/j.theochem.2004.05.012
21. Li J, Huang H, Huang Y, Dong H (2008) A theoretical study of highly nitrated azacubanes. J Energ Mat 26:230–245. https://doi.org/10.1080/07370650802182575
22. Richard RM, Ball DW (2009) Density functional calculations on the thermodynamic properties of a series of nitrosocubanes having the formula $C_8H_{8-x}(NO)x$ (x = 1−8). J Haz Mat 164:1552–1555. https://doi.org/10.1016/j.jhazmat.2008.08.057
23. Li J (2009) An evaluation of nitro derivatives of cubane using ab initio and density functional theories. Theor Chem Acc 122:101–106. https://doi.org/10.1007/s00214-008-0489-5
24. Chaban VV, Prezhdo OV (2016) Energy storage in cubane derivatives and their real-time decomposition: computational molecular dynamics and thermodynamics. ACS Energy Lett 1:189–194. https://doi.org/10.1021/acsenergylett.6b00075
25. Kiselev VG, Goldsmith CF (2019) Accurate prediction of bond dissociation energies and barrier heights for high-energy caged nitro and nitroamino compounds using a coupled cluster theory. J Phys Chem A 123:4883–4890. https://doi.org/10.1021/acs.jpca.9b01506
26. Hrovat DA, Borden WT, Eaton PE, Kahr B (2001) A computational study of the interactions among the nitro groups in octanitrocubane. J Am Chem Soc 123:1289–1293. https://doi.org/10.1021/ja001636t
27. Zhou G, Wang J, He W-D et al (2002) Theoretical investigation of four conformations of HNIW by B3LYP method. J Mol Struct

THEOCHEM 589–590:273–280. https://doi.org/10.1016/S0166-1280(02)00282-8
28. Okovytyy S, Kholod Y, Qasim M et al (2005) The mechanism of unimolecular decomposition of 2,4,6,8,10,12-hexanitro-2,4,6,8,10,12-hexaazaisowurtzitane. A computational DFT study. J Phys Chem A 109:2964–2970. https://doi.org/10.1021/jp045292v
29. Kholod Y, Okovytyy S, Kuramshina G et al (2007) An analysis of stable forms of CL-20: A DFT study of conformational transitions, infrared and Raman spectra. J Mol Struct 843:14–25. https://doi.org/10.1016/j.molstruc.2006.12.031
30. Tan B, Long X, Li J (2012) The cage strain energies of high-energy compounds. Comput Theor Chem 993:66–72. https://doi.org/10.1016/j.comptc.2012.05.033
31. Ghule VD, Jadhav PM, Patil RS et al (2010) Quantum-chemical studies on hexaazaisowurtzitanes. J Phys Chem A 114:498–503. https://doi.org/10.1021/jp9071839
32. Yang J, Wang G, Gong X et al (2018) High-energy nitramine explosives: a design strategy from linear to cyclic to caged molecules. ACS Omega 3:9739–9745. https://doi.org/10.1021/acsomega.8b00614
33. Koch E-C (2015) TEX—4,10-dinitro-2,6,8,12-tetraoxa-4,10-diazatetracyclo[5.5.0.05,9.03,11]-dodecane—review of a promising high density insensitive energetic material. Propellants Explos Pyrotech 40:374–387. https://doi.org/10.1002/prep.201400195
34. Pan Y, Zhu W, Xiao H (2017) Theoretical studies of a series of azaoxaisowurtzitane cage compounds with high explosive performance and low sensitivity. Comput Theor Chem 1114:77–86. https://doi.org/10.1016/j.comptc.2017.05.021
35. Isayev O, Gorb L, Qasim M, Leszczynski J (2008) Ab initio molecular dynamics study on the initial chemical events in nitramines: thermal decomposition of CL-20. J Phys Chem B 112:11005–11013. https://doi.org/10.1021/jp804765m
36. Kumar MA, Ashutosh P, Vargeese AA (2019) Decomposition mechanism of hexanitrohexaazaisowurtzitane (CL-20) by coupled computational and experimental study. J Phys Chem A 123:4014–4020. https://doi.org/10.1021/acs.jpca.9b01197
37. Molt RW, Bartlett RJ, Watson T, Bazanté AP (2012) Conformers of CL-20 explosive and ab initio refinement using perturbation theory: implications to detonation mechanisms. J Phys Chem A 116:12129–12135. https://doi.org/10.1021/jp305443h
38. Oliveira MAS, Borges I (2019) On the molecular origin of the sensitivity to impact of cyclic nitramines. Int J Quantum Chem 119:e25868. https://doi.org/10.1002/qua.25868
39. Ghosh M, Banerjee S, Khan MAS et al (2016) Understanding metastable phase transformation during crystallization of RDX, HMX and CL-20: experimental and DFT studies. Phys Chem Chem Phys 18:23554–23571. https://doi.org/10.1039/C6CP02185A
40. Li X-H, Zhang X-Z (2013) Computational studies on a high density cage compound hexanitrohexaazaisowurtzitane derivative. Can J Chem 91:369–374. https://doi.org/10.1139/cjc-2012-0468
41. Ju X-H, Wang Z-Y (2009) Prediction of caged polyaza polynitroamine (Tetracyclo-HMX) as energetic compound. J Energ Mat 27:133–143. https://doi.org/10.1080/07370650802405299
42. Wu Q, Zhu W, Xiao H (2013) Computer-aided design of two novel and super-high energy cage explosives: dodecanitrohexaprismane and hexanitrohexaazaprismane. RSC Adv 4:3789–3797. https://doi.org/10.1039/C3RA46625F
43. Qiu W, Ren F, Shi W, Wang Y (2015) A theoretical study on the strength of the C–NOt bond and ring strain upon the formation of the intermolecular H-bonding interaction between HF and nitro group in nitrocyclopropane, nitrocyclobutane, nitrocyclopentane or nitrocyclohexane. J Mol Model 21:114. https://doi.org/10.1007/s00894-015-2653-x
44. Wang B, Ren F, Shi W (2015) A theoretical investigation into the strength of N–NO_2 bonds, ring strain and electrostatic potential upon formation of intermolecular H-bonds between HF and the nitro group in nitrogen heterocyclic rings $C_nH_{2n}N$–NO_2 ($n = 2$–5), RDX and HMX. J Mol Model 21:302. https://doi.org/10.1007/s00894-015-2842-7
45. Du M, Wang X, Guo Z (2016) Theoretical design of bicyclo[2.2.1]heptane derivatives for high-energy density compounds with low impact sensitivity. Comput Theor Chem 1095:54–64. https://doi.org/10.1016/j.comptc.2016.09.008
46. Ren F, Cao D, Shi W, Gao H (2016) A theoretical prediction of the relationships between the impact sensitivity and electrostatic potential in strained cyclic explosive and application to H-bonded complex of nitrocyclohydrocarbon. J Mol Model 22:97. https://doi.org/10.1007/s00894-016-2967-3
47. Xiang D, Chen H, Zhu W, Xiao H (2016) Searching for a new family of high energy explosives by introducing N atoms, N-oxides, and NO_2 into a cage adamantane. Can J Chem 94:667–673. https://doi.org/10.1139/cjc-2016-0174
48. Borges I (2008) Conformations and charge distributions of diazocyclopropanes. Int J Quantum Chem 108:2615–2622. https://doi.org/10.1002/qua.21671
49. Politzer P, Lane P, Murray JS (2011) Computational characterization of a potential energetic compound: 1,3,5,7-tetranitro-2,4,6,8-tetraazacubane. Cent Eur J Energy Mater 8:39–52
50. Wiberg KB (1968) Application of the pople-santry-segal CNDO method to the cyclopropylcarbinyl and cyclobutyl cation and to bicyclobutane. Tetrahedron 24:1083–1096. https://doi.org/10.1016/0040-4020(68)88057-3
51. Harper LK, Shoaf AL, Bayse CA (2015) Predicting trigger bonds in explosive materials through Wiberg bond index analysis. ChemPhysChem 16:3886–3892. https://doi.org/10.1002/cphc.201500773
52. Shoaf AL, Bayse CA (2018) Trigger bond analysis of nitroaromatic energetic materials using Wiberg bond indices. J Comput Chem 39:1236–1248. https://doi.org/10.1002/jcc.25186
53. Shoaf AL, Bayse CA (2019) The effect of nitro groups on N_2 extrusion from aromatic azide-based energetic materials. New J Chem 43:15326–15334. https://doi.org/10.1039/C9NJ03220G
54. Cao Q (2013) Dinitroamino benzene derivatives: a class new potential high energy density compounds. J Mol Model 19:2205–2210. https://doi.org/10.1007/s00894-013-1769-0
55. Gao H, Zhang S, Ren F et al (2015) Theoretical insight into the co-crystal explosive of 2,4,6,8,10,12-hexanitrohexaazaisowurtzitane (CL-20)/1,1-diamino-2,2-dinitroethylene (FOX-7). Comput Mater Sci 107:33–41. https://doi.org/10.1016/j.commatsci.2015.05.009
56. Li X-H, Zhang R-Z, Zhang X-Z (2013) Theoretical investigations on heat of formation, detonation performance, and pyrolysis mechanism of 1,3,5,7,9,11-hexo(nitramine)-2,4,6,8,10,12- hexaazatetracyclo[5,5,0,0,0]dodecane. Can J Chem 91:1213–1218. https://doi.org/10.1139/cjc-2013-0321
57. Jeong K (2018) New theoretically predicted RDX- and -HMX-based high-energy-density molecules. Int J Quantum Chem 118:e25528. https://doi.org/10.1002/qua.25528
58. Foster JP, Weinhold F (1980) Natural hybrid orbitals. J Am Chem Soc 102:7211–7218. https://doi.org/10.1021/ja00544a007
59. Reed A, Weinhold F (1983) Natural bond orbital analysis of near-Hartree–Fock water dimer. J Chem Phys 78:4066–4073. https://doi.org/10.1063/1.445134
60. (2009) Gaussian 09. Gaussian, Inc., Wallingford, CT
61. Dunning TH (1971) Gaussian basis functions for use in molecular calculations. III. Contraction of (10s6p) atomic basis sets for the first-row atoms. J Chem Phys 55:716–723. https://doi.org/10.1063/1.1676139
62. Weigend F, Ahlrichs R (2005) Balanced basis sets of split valence, triple zeta valence and quadruple zeta valence quality for H to Rn: design and assessment of accuracy. Phys Chem Chem Phys 7:3297–3305. https://doi.org/10.1039/B508541A

63. Glendening E, Reed AE, Carpenter J, Weinhold F NBO Version 3.1
64. Politzer P, Domelsmith LN, Abrahmsen L (1984) Electrostatic potentials of strained systems: cubane, homocubane, and bishomocubane. J Phys Chem 88:1752–1758. https://doi.org/10.1021/j150653a018
65. Owens FJ (1999) Molecular orbital calculation of decomposition pathways of nitrocubanes and nitroazacubanes. J Mol Struct Theochem 460:137–140. https://doi.org/10.1016/S0166-1280(98)00312-1
66. Zhang J, Xiao H (2002) Computational studies on the infrared vibrational spectra, thermodynamic properties, detonation properties, and pyrolysis mechanism of octanitrocubane. J Chem Phys 116:10674–10683. https://doi.org/10.1063/1.1479136